NASA/TM—2011-217031

Numerical Simulations of Two-Phase Reacting Flow in a Single-Element Lean Direct Injection (LDI) Combustor Using NCC

Nan-Suey Liu
Glenn Research Center, Cleveland, Ohio

Tsan-Hsing Shih
Ohio Aerospace Institute, Brook Park, Ohio

C. Thomas Wey
Glenn Research Center, Cleveland, Ohio

July 2011

NASA STI Program . . . in Profile

Since its founding, NASA has been dedicated to the advancement of aeronautics and space science. The NASA Scientific and Technical Information (STI) program plays a key part in helping NASA maintain this important role.

The NASA STI Program operates under the auspices of the Agency Chief Information Officer. It collects, organizes, provides for archiving, and disseminates NASA's STI. The NASA STI program provides access to the NASA Aeronautics and Space Database and its public interface, the NASA Technical Reports Server, thus providing one of the largest collections of aeronautical and space science STI in the world. Results are published in both non-NASA channels and by NASA in the NASA STI Report Series, which includes the following report types:

- TECHNICAL PUBLICATION. Reports of completed research or a major significant phase of research that present the results of NASA programs and include extensive data or theoretical analysis. Includes compilations of significant scientific and technical data and information deemed to be of continuing reference value. NASA counterpart of peer-reviewed formal professional papers but has less stringent limitations on manuscript length and extent of graphic presentations.

- TECHNICAL MEMORANDUM. Scientific and technical findings that are preliminary or of specialized interest, e.g., quick release reports, working papers, and bibliographies that contain minimal annotation. Does not contain extensive analysis.

- CONTRACTOR REPORT. Scientific and technical findings by NASA-sponsored contractors and grantees.

- CONFERENCE PUBLICATION. Collected papers from scientific and technical conferences, symposia, seminars, or other meetings sponsored or cosponsored by NASA.

- SPECIAL PUBLICATION. Scientific, technical, or historical information from NASA programs, projects, and missions, often concerned with subjects having substantial public interest.

- TECHNICAL TRANSLATION. English-language translations of foreign scientific and technical material pertinent to NASA's mission.

Specialized services also include creating custom thesauri, building customized databases, organizing and publishing research results.

For more information about the NASA STI program, see the following:

- Access the NASA STI program home page at *http://www.sti.nasa.gov*

- E-mail your question via the Internet to *help@sti.nasa.gov*

- Fax your question to the NASA STI Help Desk at 443–757–5803

- Telephone the NASA STI Help Desk at 443–757–5802

- Write to:
  NASA Center for AeroSpace Information (CASI)
  7115 Standard Drive
  Hanover, MD 21076–1320

NASA/TM—2011-217031

Numerical Simulations of Two-Phase Reacting Flow in a Single-Element Lean Direct Injection (LDI) Combustor Using NCC

Nan-Suey Liu
Glenn Research Center, Cleveland, Ohio

Tsan-Hsing Shih
Ohio Aerospace Institute, Brook Park, Ohio

C. Thomas Wey
Glenn Research Center, Cleveland, Ohio

National Aeronautics and
Space Administration

Glenn Research Center
Cleveland, Ohio 44135

July 2011

Acknowledgments

This work has been supported by the Subsonic Fixed Wing Project and the Supersonics Project under the NASA Fundamental Aeronautics Program.

This report is a formal draft or working paper, intended to solicit comments and ideas from a technical peer group.

This report contains preliminary findings, subject to revision as analysis proceeds.

This work was sponsored by the Fundamental Aeronautics Program at the NASA Glenn Research Center.

Level of Review: This material has been technically reviewed by technical management.

Available from

NASA Center for Aerospace Information
7115 Standard Drive
Hanover, MD 21076–1320

National Technical Information Service
5301 Shawnee Road
Alexandria, VA 22312

Available electronically at http://www.sti.nasa.gov

Numerical Simulations of Two-Phase Reacting Flow in a Single-Element Lean Direct Injection (LDI) Combustor Using NCC

Nan-Suey Liu
National Aeronautics and Space Administration
Glenn Research Center
Cleveland, Ohio 44135

Tsan-Hsing Shih
Ohio Aerospace Institute
Brook Park, Ohio 44142

C. Thomas Wey
National Aeronautics and Space Administration
Glenn Research Center
Cleveland, Ohio 44135

Abstract

A series of numerical simulations of Jet-A spray reacting flow in a single-element lean direct injection (LDI) combustor have been conducted by using the National Combustion Code (NCC). The simulations have been carried out using the time filtered Navier-Stokes (TFNS) approach ranging from the steady Reynolds-averaged Navier-Stokes (RANS), unsteady RANS (URANS), to the dynamic flow structure simulation (DFS). The sub-grid model employed for turbulent mixing and combustion includes the well-mixed model, the linear eddy mixing (LEM) model, and the filtered mass density function (FDF/PDF) model. The starting condition of the injected liquid spray is specified via empirical droplet size correlation, and a five-species single-step global reduced mechanism is employed for fuel chemistry. All the calculations use the same grid whose resolution is of the RANS type. Comparisons of results from various models are presented.

1.0 Introduction

A prerequisite for accurate prediction of turbulent combustion in the combustor is the ability of the turbulence model to capture the unsteady turbulent structures responsible for the mixing in the combustor. Approaches such as the large eddy simulation (LES) and the time filtered Navier-Stokes simulation (TFNS) are capable of capturing the dynamically important, unsteady turbulent flow structures. In the case of LES, the filtered equations are established by applying a spatial filter to the exact form of the governing equations. The filter width is typically the local grid size; in addition, the eddy viscosity has the local grid size as a model parameter. Therefore, the grid resolution and the model fidelity are formally linked, and, in principal, a grid independent solution cannot be cleanly reached. In the case of TFNS, the filtered equations are established by applying a temporal filter to the exact form of the governing equations. The filter width does not relate to the time step of the numerical solution, and the eddy viscosity contains the so called "resolution control parameter" which is conceptually defined as the ratio of the temporal filter width to a characteristic integral time scale. Since the grid resolution and the model fidelity are not formally linked, in principal, a grid independent solution can be unambiguously attained. It should be pointed out that TFNS is not LES, nor hybrid RANS/LES, nor, in general, unsteady Reynolds-averaged Navier-Stokes (URANS). In our previous reports (e.g., Ref. 1), the TFNS was known as the partially resolved numerical simulation (PRNS) and the dynamic flow structure simulation (DFS) as the very large eddy simulation (VLES). In the present report, TFNS/DFS and PRNS/VLES are interchangeable.

Turbulent combustion also requires modeling the turbulence-chemistry interaction process. To this end, various sub-grid combustion models have been invoked, e.g., well-mixed model, eddy-break-up model (EBU) (Ref. 2), thickened flame model (Ref. 3), flamelet-based model (Ref. 4), conditional moment closure method (CMC) (Ref. 5), filtered mass density function/probability density function method (FDF/PDF) (Ref. 6), and linear eddy mixing model (LEM) (Ref. 7). In the well-mixed model, the distributions of scalars within a CFD computational cell are assumed to be homogeneous, i.e., their values equal to their respective mean values provided by the CFD solution of the filtered equations. The well-mixed model is often used in the direct numerical simulation (DNS).

Fuel chemistry models ranging from global reduced mechanism involving a few species and reaction steps to detailed mechanism involving several hundreds of species and reaction steps exist. Global reactions are computationally less intensive, but they lack emissions and extinction information. Kinetics calculations using detailed mechanism consume long CPU time as well as large computer memory; hence, they are rarely, if ever, performed on the flight during the simulation. Typically, libraries of pre-computed tables are established by using detailed mechanism, then, linked to the simulation through interpolation procedure. Tabulation strategy such as the artificial neural network (ANN) has been used to further speed up the kinetics calculations while reducing the memory requirement (Ref. 8).

For liquid fueled combustion, models for primary atomization, secondary droplet breakup, droplet vaporization, and droplet transportation are needed. The performance of these models directly impacts the local fuel vapor distribution in the calculated combustion field, therefore, can play a major role in the overall accuracy of the prediction. Last, but not the least, surrogate of the targeted fuel, e.g., the Jet-A, and its transport properties as well as its chemical kinetics should also be determined.

The objective of this report is to summarize the calculated results from a series of numerical simulations of two-phase reacting flow in a single-element lean direct injection (LDI) combustor using the National Combustion Code (NCC). The NCC is a NASA in-house code for the modeling and simulation of multi-phase turbulent combustion in combustors (Ref. 9). The LDI concept has the potential for low emissions under operational (high temperature, high pressure) conditions. In this concept, the liquid fuel is injected from a venturi directly into the incoming swirling airflow, and the swirling airstream is used to atomize the injected liquid as well as to promote fuel-air mixing (Ref. 10). The flame structure can be very complex and locally range from non-premixed to premixed burning.

This report is organized as follows. In the next section, a description of the TFNS formulation of two-phase flow and the candidate sub-grid combustion models are presented. In Section 3, some features of the experimental and computational setup are highlighted. This is followed by comparisons between measured data and computed results, and the concluding remarks.

2.0 Formulation

The conservation equations for compressible reacting flow are solved using the TFNS approach. To simulate spray combustion, Lagrangian droplet model is concurrently solved with the Eulerian gas flow.

2.1 Gas Phase

2.1.1 Governing Equations for Time Filtered Field

Using the TFNS/DFS (previously known as PRNS/VLES) approach detailed in Reference 1, the following filtered equations are obtained,

2.1.1.1 Continuity and Momentum Equations

$$\overline{\rho}_{,t} + \left(\overline{\rho}\,\tilde{u}_i\right)_{,i} = 0, \quad \overline{p} = \overline{\rho} R \tilde{T} \tag{1}$$

$$\left(\overline{\rho}\tilde{u}_i\right)_{,t}+\left(\overline{\rho}\tilde{u}_i\tilde{u}_j\right)_{,j}=-\left(\overline{p}+\frac{1}{3}\tau_{kk}\right)_{,i}+\left(2\left(\overline{\mu}+\mu_T\right)\tilde{s}_{ij}-\frac{2}{3}\delta_{ij}\left(\overline{\mu}+\mu_T\right)\tilde{s}_{kk}\right)_{,j}+S_i^T \tag{2}$$

where

$$\mu_T=f_1 C_\mu \overline{\rho}\frac{k^2}{\varepsilon} \tag{3}$$

$$\begin{aligned} S_i^T=&\left\{A_3 f_3 \overline{\rho}\frac{k^3}{\varepsilon^2}\left(\tilde{s}_{ik}\tilde{\omega}_{kj}-\tilde{\omega}_{ik}\tilde{s}_{kj}\right)\right\}_{,j}\\ &-\left\{2A_5 f_5 \overline{\rho}\frac{k^4}{\varepsilon^3}\left[\tilde{\omega}_{ik}\tilde{s}_{kj}^2-\tilde{s}_{ik}^2\tilde{\omega}_{kj}+\tilde{\omega}_{ik}\tilde{s}_{km}\tilde{\omega}_{mj}-\tilde{\omega}_{kl}\tilde{s}_{lm}\tilde{\omega}_{mk}\delta_{ij}+II_s(\tilde{s}_{ij}-\delta_{ij}\tilde{s}_{kk}/3)\right]\right\}_{,j}\end{aligned} \tag{4}$$

$$f_i\left(\frac{\Delta_T}{T}\right)\approx 2\left(\frac{\Delta_T}{T}\right)-\left(\frac{\Delta_T}{T}\right)^2 \qquad i=1,3,5 \tag{5}$$

We call the ratio Δ_T/T the resolution control parameter (RCP). It controls, conceptually at the governing equation level, the time scales content of the unsteady flow structures targeted for capturing in the practical numerical solution.

When $RCP \rightarrow 1.0$, all time scales of fluctuations (turbulence) have been filtered, and the TFNS simulation is a de facto RANS simulation, i.e., the directly calculated field is intrinsically the time mean, no turbulent fluctuation occurs in the directly calculated quantities. As the value of *RCP* decreases, the unsteady fluctuations will become more pronounced in the directly calculated field, if the grid sizes are adequate. To perform a TFNS simulation, we need to choose a value of *RCP* from the outset. The following relationship suggests a way to guide the selection of the value of *RCP*:

$$RCP=\frac{\Delta_T}{T}\sim\frac{\overline{k}/\overline{\varepsilon}}{k_{ref}/\varepsilon_{ref}}\sim\frac{\overline{k}}{k_{ref}} \tag{6}$$

For example, *RCP* = 0.3 means that we intend to directly calculate (i.e., to capture) flow structures associated with time scales responsible for about 70 percent of the total fluctuating (turbulent) kinetic energy, and the rest 30 percent of the total turbulent kinetic energy will be accounted for by the modeled sub-filter kinetic energy.

2.1.1.2 Transport Equations for Sub-Filter *k*–ε

$$\frac{\partial}{\partial t}\overline{\rho}k+\frac{\partial}{\partial x_i}\overline{\rho}\tilde{u}_i k=\frac{\partial}{\partial x_i}\left[\left(\overline{\mu}+\mu_T\right)\frac{\partial}{\partial x_i}k\right]-\tau_{ij}\tilde{s}_{ij}-\overline{\rho}\varepsilon \tag{7}$$

$$\frac{\partial}{\partial t}\overline{\rho}\varepsilon+\frac{\partial}{\partial x_i}\overline{\rho}\tilde{u}_i \varepsilon=\frac{\partial}{\partial x_i}\left[\left(\overline{\mu}+\mu_T\right)\frac{\partial}{\partial x_i}\varepsilon\right]-C_{\varepsilon 1}\tau_{ij}\tilde{s}_{ij}\frac{\varepsilon}{k}-C_{\varepsilon 2}\frac{\overline{\rho}\varepsilon^2}{k} \tag{8}$$

2.1.1.3 Energy and Species Equations

$$\frac{\partial \overline{\rho}\,\tilde{e}}{\partial t}+\frac{\partial \overline{\rho}\,\widetilde{U_i e}}{\partial x_i}=-\frac{\partial \overline{q}_i}{\partial x_i}+\overline{PS_{kk}}+\overline{\rho}\,\tilde{\varepsilon}+\overline{Q} \tag{9}$$

$$\frac{\partial \overline{\rho}\,\widetilde{\Phi}_m}{\partial t}+\frac{\partial \overline{\rho}\,\widetilde{U_i\Phi_m}}{\partial x_i}=\frac{\partial}{\partial x_i}\left(\Gamma^{(m)}\frac{\partial \overline{\rho}\,\widetilde{\Phi}_m}{\partial x_i}\right)+\overline{\rho}\,\tilde{S}_m \qquad m=1,2,\cdots,N \tag{10}$$

where

$$\overline{\rho}\,\widetilde{U_i\Phi_m}=\overline{\rho}\,\widetilde{U}_i\widetilde{\Phi}_m-\Gamma_T^{(m)}\frac{\partial \overline{\rho}\,\widetilde{\Phi}_m}{\partial x_i}-\Gamma_T^{(m)}\frac{k}{\varepsilon}\left(c_1\tilde{S}_{ij}+c_2\widetilde{\Omega}_{ij}\right)\frac{\partial \overline{\rho}\,\widetilde{\Phi}_m}{\partial x_j} \tag{11}$$

$\overline{\rho}\,\widetilde{U_i e}$ has the same form as $\overline{\rho}\,\widetilde{U_i\Phi}_m$, except that Φ_i is replaced by *e*, and the turbulent species diffusivity is replaced by turbulent heat conductivity.

and

$$\overline{q}_i=-\kappa c_\upsilon\frac{\partial \overline{\rho}\,\tilde{T}}{\partial x_i} \tag{12}$$

2.1.2 Models for Sub-Grid Mixing and Combustion

2.1.2.1 Well-Mixed Model

In well-mixed model, the distributions of scalars within a CFD computational cell are assumed to be homogeneous, i.e., their values equal to their respective mean values provided by the CFD solution of the filtered equations. Therefore, the filtered reaction rates are directly calculated using the filtered species mass fractions and filtered temperature defined at the computational cell center. The well-mixed model is, at the best, valid only in cells in which the sub-grid fluctuations are physically low.

2.1.2.2 Linear-Eddy Mixing (LEM) Model

The LEM model (Ref. 7) is implemented in terms of a fractional splitting technique; it is divided into two processes: sub-grid and super-grid. The super-grid process emulates the convection of the scalar field by the grid-resolved velocity field across the surfaces of the computational cell. The sub-grid process, which occurs within each computational cell, consists of four operators: (a) molecular diffusion, (b) finite-rate kinetics, (c) volumetric expansion caused by the heat release, and (d) stochastic stirring due to the sub-grid eddies.

2.1.2.2.1 Sub-Grid Process

Within each CFD computational cell, a one-dimensional domain consisting of a fixed number of LEM elements is employed, the governing equations have the following form:

Species equation

$$\frac{dY_i}{dt} = \frac{\dot{w}_i'''}{\rho_\ell} - C_\phi \omega \left(Y_i - \overline{Y}_i \right) + S_{mls} \tag{13}$$

Energy equation

$$\frac{dh_\ell}{dt} = -C_\phi \omega \left(h_\ell - \overline{h} \right) + S_{mle} \tag{14}$$

$F_{T,\text{stirring}}$ and $F_{Y_i,\text{stirring}}$ represent the sub-grid turbulent mixing, and they are accounted for by employing a stochastic rearrangement of the LEM elements, known as the triplet mapping. This mapping, which mimics the characteristics of the stirring process inherent to turbulent flows, have three parameters: the stirring frequency λ, a notional (stirring) eddy of size fi, and its stirring position on the linear LEM elements. The stirring position is randomly chosen from a uniform distribution. The eddy size is randomly selected from a prescribed distribution function given by

$$f(l) = (5/3) l^{-8/3} \Big/ \left[\eta^{-5/3} - l_t^{-5/3} \right] \tag{15}$$

Here, the Kolmogorov length scale η is estimated via $\eta \sim l_t \, \mathrm{Re}^{-3/4}$, and l_t is the integral length scale of the turbulence. The event rate (frequency per unit length) is determined from

$$\lambda = \frac{54}{5} \frac{v \, \mathrm{Re}_t}{C_\lambda l_t^3} \frac{\left[(l_t/\eta)^{5/3} - 1 \right]}{\left[1 - (\eta/l_t)^{4/3} \right]} \tag{16}$$

The stirring time interval between events is given by $\Delta t_{\text{stir}} = 1/(\lambda \Delta)$ where Δ is the length of the one-dimensional LEM domain in a CFD computational cell.

2.1.2.2.2 Super-Grid Process

The grid-resolved convection of the scalar field is implemented by a Lagrangian transfer of LEM elements across the surfaces of the CFD computational cells. This Lagrangian transport is also known as splicing. Referring to Figure 1, for example, the outward mass through the right side of a cell computed from resolved velocity and density is equivalent to 1.5 LEM elements and colored in red. The outward mass through the bottom side of the mesh is equivalent to 2.5 LEM elements and colored in magenta. Similarly, the inward mass through the top and left sides of the mesh are equivalent to 6 LEM elements. Splicing will result in e.g., 14 LEM elements in this computational cell. In general, splicing will cause different computational cell to have different number of LEM elements. To avoid programming complexities in a parallel environment, the LEM domain is regridded to have the same fixed number of elements, and each element is of the same volume. Conservation of mass is maintained during regridding.

In general, the LEM module receives the filtered velocity, pressure and turbulence fields from the CFD flow module. It also receives the source terms due to the liquid-phase contribution from the spray module. However, the feedback from the LEM module to the CFD flow module can be accomplished in several ways. In this report, the LEM module provides the species and the temperature fields to the CFD flow module and the spray module. Other feedback alternatives are currently being investigated.

2.1.2.3 Filtered Mass Density Function (FDF/PDF) Model

Under the present effort, the FDF/PDF model is implemented using an Eulerian Monte Carlo method (Refs. 11 and 12). The transport equation of FDF is solved by making use of an approximate factorization scheme. It is split into four operators respectively associated with the chemical reactions, the molecular mixing, the spray and the convection. In the Monte Carlo simulation, the filtered density function is represented by an ensemble of stochastic particles. Each particle carries enthalpy, temperature and species mass fractions.

2.1.2.3.1 Sub-Grid Process

For each notional particle, the following equations are solved:

Species equation

$$\frac{dY_i}{dt} = \frac{\dot{w}_i'''}{\rho_\ell} - C_\phi \omega \left(Y_i - \overline{Y}i \right) + S_{mls} \tag{17}$$

Energy equation

$$\frac{dh_\ell}{dt} = -C_\phi \omega \left(h_\ell - \overline{h} \right) + S_{mle} \tag{18}$$

where $\omega = \varepsilon/k$, C_ϕ, is an empirical constant. The first term on the right hand side of the energy equation accounts for the molecular mixing by making use of the relaxation to the ensemble mean. The last term, S_{mle} represents the contribution from the spray source terms.

2.1.2.3.2 Super-Grid Process

The grid-resolved convection of the scalar field is implemented in an Eulerian context. Referring to Figure 2, unlike the LEM splicing algorithm, the Eulerian convection and diffusion process is achieved through the content replacement of particles, as each Monte Carlo particle carries the information of the mass fraction of species, the enthalpy, the temperature, but not the volume. For example, the outward mass through the right side of a cell, computed from the grid-resolved velocity and density; and normalized by the mass in the cell, is equal to 5 percent and colored in red. The outward mass through the bottom side of the mesh is equal to 10 percent and colored in magenta. Similarly, the inward mass through the top and left sides of the mesh are equivalent to 40 percent and colored in dark and light green. If the total number of the particles is 20 in this cell, then one particle (5 percent of 20) will be randomly selected from its right adjacent cell, and its contents are copied to one randomly selected particle in the current cell. The same procedure is applied to other particles in colors. For those remaining particles (45 percent here) the contents are randomly shuffled within the cell.

In general, the FDF/PDF module receives the filtered velocity, pressure and turbulence fields from the CFD flow module. It also receives the source terms due to the liquid-phase contribution from the spray module. However, the feedback from the FDF/PDF module to the CFD flow module can be accomplished in several ways. In this report, the FDF/PDF module provides the species and the temperature fields to the CFD flow module and the spray module. Other feedback alternatives are currently being investigated.

2.2 Liquid Phase

The governing equations for the liquid phase are based on a Lagrangian formulation where the spray particle position and velocity are described by a set of ordinary differential equations. Various sub-models, such as the droplet drag model and the drop vaporization model, are needed to simulate the transport of a vaporizing spray particle. The specification of the fuel injector exit condition plays a major role in the fidelity of the simulation. Common practice is to specify the starting droplet condition using correlations of droplet sizes calibrated by relevant experimental data. In addition to the use of correlation, various models for primary atomization and secondary droplet breakup have been implemented into the NCC and evaluated/validated. A more detailed description of the liquid phase modeling and the coupling between the liquid and gas phase transport can be found in References 13 and 14.

3.0 Experimental and Computational Setup

The single-element LDI combustor is illustrated in Figure 3, more detailed description of the combustor geometry and the test rig can be found in Reference 15. Each element consists of an air passage with an upstream air swirler and a converging-diverging venturi section. The fuel is injected through the center of swirler and the fuel tip is at the throat of the venture. The air swirlers have six helical, axial vanes with downstream vane angles of 60°. The air then dumps into a combustion chamber with a square cross-section. Velocity measurements were taken with a two-component Laser Doppler Velociometry (LDV) system, temperature measurements were taken with thermocouples, and emissions data was gathered via an isokinetic probe and gas analyzer. Quartz makes up the combustion section. The combustor experiments may have significant convective and radiation heat losses. The temperature measurements reported are not corrected to adiabatic conditions. Experimental droplet measurements are collected with a Phase Doppler Particle Analyzer (PDPA).

The computational domain consists of approximately 862,000 hexahedral elements (Fig. 3). At the air inflow boundary, the air flow speed is 20.14 m/s, the density is 1.19 Kg/m, and the static temperature is 294.28 K. At the combustor chamber exit, static pressure is specified for the steady RANS calculations, while convective conditions are used for the URANS and PRNS calculations. The operating pressure of the combustor is approximately 1 atm, and the measured pressure drop (as a percentage of the air inlet pressure) during the experiments was measured at 4 percent.

The fuel is injected at 0.415 g/s, which gives a global equivalence ratio of 0.75. The specification of the starting condition for the fuel spray is particularly critical for accurate predictions. In this study, the following droplet size distribution is used (Ref. 13):

$$\frac{dn}{n} = 4.21\times10^{6}\left[\frac{d}{d_{32}}\right]^{3.5} e^{-16.98\left(\frac{d}{d_{32}}\right)^{0.4}} \frac{dd}{d_{32}} \tag{19}$$

Where n is the total number of the droplets and dn is the number of droplets in the size range between d and $d+dd$. This correlation also requires the specification of a Sauter mean diameter, d_{32} and the number of droplet classes. These specified inflow droplets will undergo evaporation without secondary breakup. Experimental data suggests a Sauter mean diameter around 32 μm, and the spray cone angle is 90°.

In this study, the liquid fuel $C_{12}H_{23}$ is used as the surrogate for the experimental Jet-A fuel, and a single-step, five-species global reduced mechanism (see e.g., Ref. 16) is employed for the chemical reactions Table 1.

4.0 Results

The National Combustion Code (NCC) has been used for all the calculations. The results of the non-reacting flows and the comparison with the experimental data can be found in Reference 17, and they reveal the dominant flow structures in the LDI combustor.

Figure 4 is a snapshot of the unsteady flow field. Embedded in this figure are the instantaneous iso-surface of the zero axial velocity component colored by the effective eddy viscosity and six instantaneous stream lines emanating from the upstream of the swirler, going through the converging-diverging nozzle, then passing through the combustion chamber.

The dominant flow structures in the LDI combustor can be best visualized via the iso-surface of the zero axial velocity and the iso-surface of a relatively low pressure. The iso-surface of the zero axial velocity is also known as the vortex breakdown bubble (VBB). The iso-surface of a sufficiently low pressure captures the precessing vortex core (PVC).

Figure 5 is a snap shot of the PVC and VBB. The dark blue region is a vortex core, which is formed near the venturi throat and extends into the combustor chamber. This spiraling vortex core rotates and breaks, it changes randomly in space and time. Embedded in this figure is an instantaneous stream line, which starts from the upstream of the swirler and goes through a complex, seemingly random path in the combustor chamber. This stream line spirals around the dark blue surface indicating that the dark blue region is indeed a vortex core. The light green surfaces are the iso-surfaces of the zero axial velocity. In addition to the VBB, there are some small structures near the dump plane and in the corner region. It is very reasonable to expect that the dynamics of the PVC and the VBB, as well as their interactions, are critical to the fuel-air mixing and the flame stability in the LDI combustors.

The same grid is used for the two-phase reacting flow calculations. Figure 6 is a snapshot of the spray droplet field. In the following, we first report results from RANS, URANS, PRNS (all using the well-mixed model) and comparison with measured data, then the results from PRNS using different sub-grid models (LEM and FDF/PDF) and comparison with measured data. Due to the uncertainty in the imposed starting condition of the spray, the use of a simple single-step global chemistry model, and the yet to be optimized coupling between the CFD flow module and the LEM or FDF/PDF module in the framework of the time filtered Navier-Stokes simulation, the currently reported results and comparison with data should be viewed as preliminary. Results from refined simulations will be reported in the future.

4.1 RANS, URANS, and PRNS Using Well-Mixed Model

The steady state RANS (RCP = 1.0) solution is obtained by an iteration procedure using a Runge-Kutta scheme, and the static pressure is imposed at the outlet boundary of the computational domain. The unsteady URANS (RCP = 1.0) and PRNS (RCP = 0.26) solutions are obtained by a second order time accurate, iteratively implicit algorithm, and the outlet boundary condition facilitates the convection of pressure disturbances out of the computational domain. In this Section, the well-mixed model is employed to provide the filtered reaction source terms in the filtered species equations, i.e., the scalar field of the overall simulation is determined from the solution of the filtered energy and species equations of the finite-volume CFD module.

Figure 7 presents the contours of the time averaged axial velocity in the center plane, while the time averaged temperature contours are shown in Figure 8. There are differences in the strength and extent of the center recirculation region and the corner vortex. More pronounced is the temperature difference in the flame zone. Figure 9 shows the comparison of the time averaged axial velocity along the center line. Comparisons of the time averaged axial velocity at several downstream cross-sections are presented in Figures 10 and 11. Comparisons of the time averaged temperature are given in Figures 12 to 14.

4.2 PRNS Using LEM and FDF/PDF Models

For this set of calculations, the starting condition is an instantaneous solution of the PRNS using well-mixed model. Figure 15 depicts the starting condition in the center plane. With this starting field, the unsteady MacCormack scheme is chosen to continue the PRNS calculation using either LEM model or FDF/PDF model. When the LEM model is employed, 24 LEM elements per CFD computational cell are used, and up to 40 stirring events and reaction-diffusion operations are imposed over one CFD flow time step, rather than dynamically determined from the diffusion time scales and the correlation for the stirring events (see Section 2.1.2). When the FDF/PDF model is employed, 100 Monte Carlo particles per CFD computational cell are used, and a weighted time averaging scheme is adopted to reduce the statistical noise. In these two cases, unlike when the well-mixed model is employed, the scalar fields (i.e., temperature and species mass fractions) of the overall simulation are provided by the solution of the LEM module or the FDF module, while the velocity and pressure fields of the overall simulation are provided by the finite-volume CFD module.

Figure 16 presents the contours of the time averaged axial velocity, temperature and fuel vapor mass fraction in the center plane obtained from LEM/PRNS. Figure 17 shows the time averaged axial velocity, temperature and fuel vapor mass fraction in the center plane obtained from FDF/PRNS. These two models result in quite different time averaged patterns.

In the following, comparisons of time averaged results among LEM/PRNS, FDF/PRNS and the experiment are presented. The starting condition (denoted as well-mixed/PRNS) is also included for reference. The comparison of time averaged axial velocity along the center line is shown in Figure 18, the comparison of time averaged temperature along the center line is given in Figure 19. The time averaged temperature; axial velocity and azimuth velocity at several downstream stations are presented in Figures 20 to 22, respectively. Generally speaking, the comparisons do not suggest good agreement among the results. Some of the major contributing factors have been briefly mentioned above; the role of the CFD grid size in the performance of these sub-grid models also needs to be assessed.

5.0 Concluding Remarks

Numerical simulations of two-phase reacting flow in a single-element LDI combustor have been carried out using the time filtered Navier-Stotkes (TFNS) approach ranging from steady Reynolds averaged Navier-Stokes (RANS), unsteady RANS (URANS), to dynamic flow structure simulation (DFS). The TFNS/DFS is previously known as the PRNS/VLES. Results are obtained by employing different sub-grid mixing and combustion models, namely, well-mixed, LEM and FDF/PDF. All the calculations use the same grid whose resolution is of the RANS type. The present results should be considered as preliminary, because of the uncertainty in the imposed starting condition for the spray, the use of a five-species single-step global chemistry model, and the yet to be optimized coupling between the CFD finite-volume module and the LEM or FDF/PDF module. The role of the grid size in the performance of these sub-grid models also needs to be assessed. These issues are currently being addressed.

References

1. Shih, T.-H. and Liu, N.-S., “A Nonlinear Dynamic Subscale Model for PRNS/VLES of Internal Combustor Flows,” AIAA–2009–0467, January 4–January 8, 2009, Orlando, FL.
2. Kirtas, M., Patel, N., Sankaran, V. and Menon, S., “Large-eddy Simulation of a Swirl-stabilized, Lean Direct Injection Spray Combustor,” Proceedings of ASME GT2006, May 8–11, 2006, Barcelona, Spain.
3. Legier, J.P., Poinsot, T. and Veynante, D., “Dynamically Thickened Flame LES model for Premixed and Non-premixed Turbulent Combustion,” Proceedings of the Summer Program 2000, Center for Turbulence Research, Stanford University, pp. 157–168.

4. Knudsen, E. and Pitsch, H., "Large Eddy Simulation of a Spray Combustor Using a Multi-regime Flamelet Approach," Annual Research Briefs 2010, Center for Turbulence Research, Stanford University, pp. 337–350.
5. Sreedhara, S. and Huh, K.Y., "Assessment of Closure Schemes in Second-Order Conditional Moment Closure against DNS with Extinction and Ignition," Combustion and Flame 143 (2005) 386–401.
6. James, S., Zhu, J. and Anand, M.S., "Large Eddy Simulations of Turbulent Flames Using the Filtered Density Function Model," Proceedings of the Combustion Institute 31 (2007) 1737–1745.
7. Patel, N., and Suresh, M., "Simulation of Spray-Turbulence-Flame Interactions in a Lean Direct Injection Combustor," Combustion and Flame 153 (2008) 228–257.
8. Sen, B.A., Hawkes, E.R. and Menon, S., "Large Eddy Simulation of Extinction and Reignition with Artificial Neural Networks Based Chemical Kinetics," Combustion and Flame 157 (2010) 566–578.
9. Liu, N.-S., Shih, T.-H. and Wey, T., "Comprehensive Combustion Modeling and Simulation: Recent Progress at NASA Glenn Research Center," ISABE-2007-1268, 18th International Symposium on Air Breathing Engines, September 2–7, 2007, Beijing, China.
10. Hicks, Y.R., Anderson, R.C. and Locke, R.J., "Optical Measurements in a Combustor Using a 9-Point Swirl-Venturi Fuel Injector," ISABE-2007-1280, 18th International Symposium on Air Breathing Engines, September 2–7, 2007, Beijing, China.
11. Raju, M.S., "Current Status of the Overall Spray Solution Procedure (Combined CFD/Scalar-Monye-Carlo-PDF/Spray Computations) Developed under NCC," AIAA–2004–0327, 42nd AIAA Aerospace Sciences Meeting and Exhibit, 5–8 January 2004, Reno, NV.
12. Shih, T.-H. and Liu, N.-S., "Density Weighted FDF Equations for Simulations of Turbulent Reacting Flows," NASA/TM—2011-217012, 2011.
13. Raju, M.S., "LSPRAY-III: A Lagrangian Spray Module," NASA/CR—2008-215290, 2008.
14. Raju, M.S. and Bulzan, D., "Assessment of Atomization Models Used in Spray Calculations," NASA/TM, 2011. (submitted)
15. Cai, J., Jeng, S.-M., and Tacina, R., "The Structure of a Swirl-Stabilized Reacting Spray Issued from an Axial Swirler," AIAA–2005–1424, 43rd AIAA Aerospace Science Meeting and Exhibit, 10–13 January 2005, Reno, NV.
16. Iannetti, A.C. and Liu, N.-S., "The Effect of Spray Initial Conditions on Heat Release and Emissions in LDI CFD Calculations," AIAA–2008–1150, 46th AIAA Aerospace Science Meeting and Exhibit, 7–10 January 2008, Reno, NV.
17. Liu, N.-S. and Shih, T.-H., "A Very Large Eddy Simulation of the Non-reacting Flow in a Single-Element Lean Direct Injection Combustor Using PRNS with a Nonlinear Subscale Model," ISROMAC-13-36, Proceedings of the 13th International Symposium on Transport Phenomena and Dynamics of Rotating Machinery, 4–9 April 2010, Honolulu, HI.

TABLE 1.—SINGLE STEP (GLOBAL) CHEMISTRY MODEL

	Reaction	a (mole-cm-sec-k)	n	E (cal/mole)
1	**4 C12H23+71 O2=> 48 CO2 + 46 H20** GLO/C12H23 0.10/ GLO/O2 1.65/	8.60E+11	0.00	3.00E+4

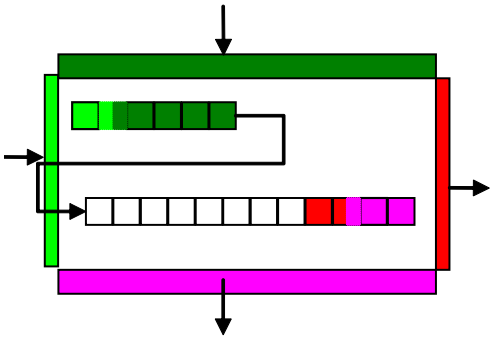

Arrows -- Convection direction
Initial number of lumps – 12
Light Green – inward mass (1.5)
Dark Green – inward mass (4.5)
Red – outward mass (1.5)
Magenta – outward mass (2.5)
Current number of lumps -- 14
Final number of lumps will became 12 after re-gridding via equalizing the volume.

Figure 1.—Schematic illustrating the splicing algorithm used for scalar convection. (Assuming number of LEM elements is 12. Each element carries its own volume and species density).

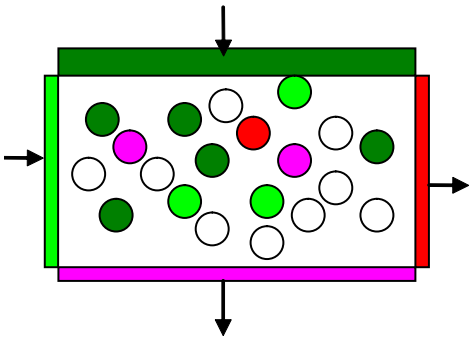

Arrows -- Convection direction
Light Green – inward mass (15%=3)
Dark Green – inward mass (25%=5)
Red – outward mass (5%=1)
Magenta – outward mass (10%=2)
Number of Monte Carlo particles – 20
Contents of randomly selected particles are replaced by those of randomly selected particles from adjacent cells.

Figure 2.—Schematic illustrating the process of the scalar convection and diffusion for the Eulerian Monte Carlo FDF/PDF model.

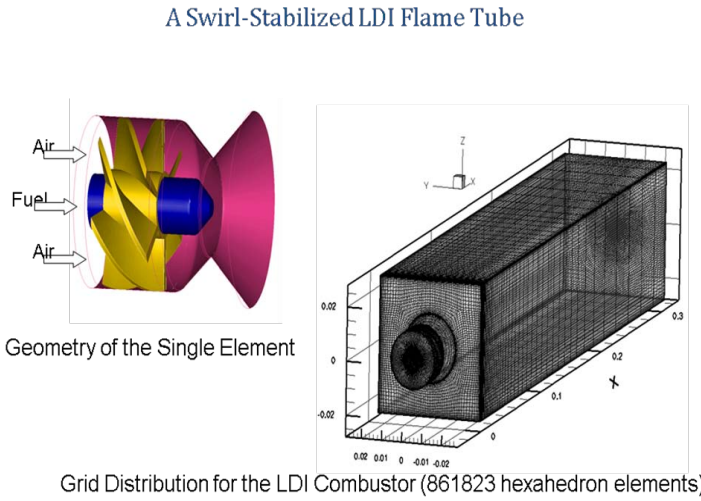

Figure 3.—Swirler geometry and computational domain for the LDI combustor.

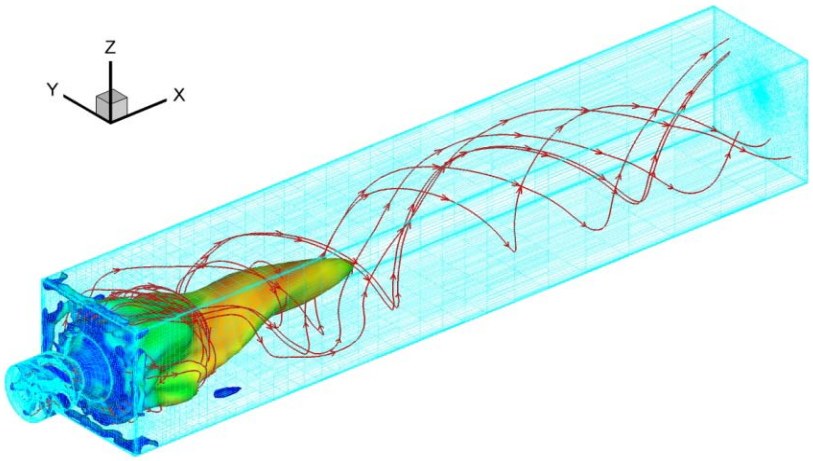

Figure 4.—A snapshot of the flow field from the PRNS simulation.

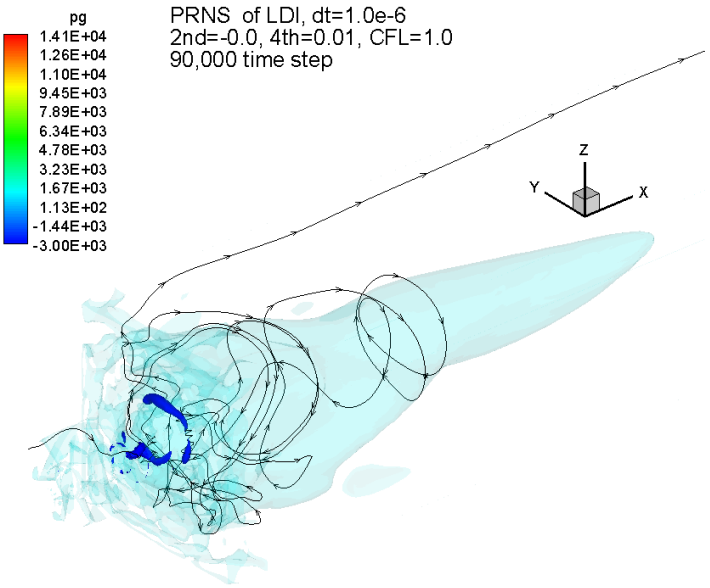

Figure 5.—A snapshot of the flow structures: precessing vortex core (PVC) and vortex breakdown bubble (VBB).

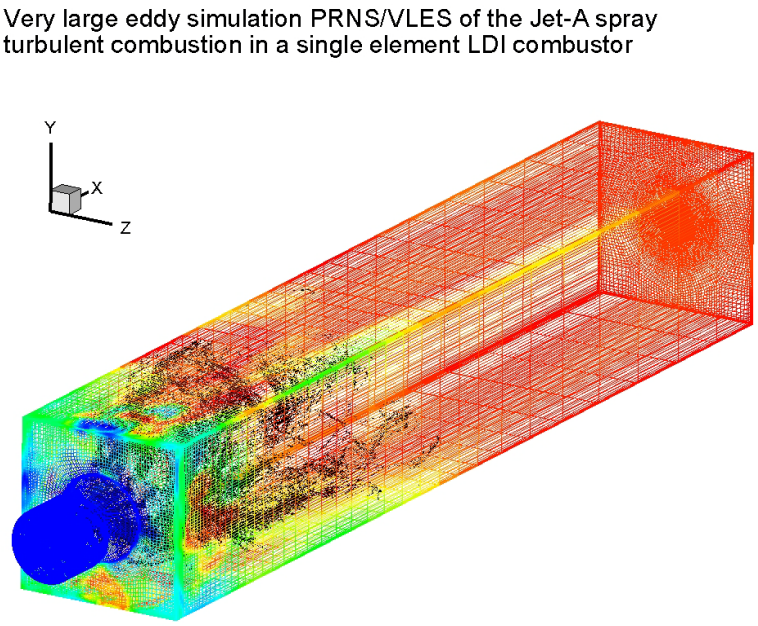

Figure 6.—A snapshot of the spray droplet field.

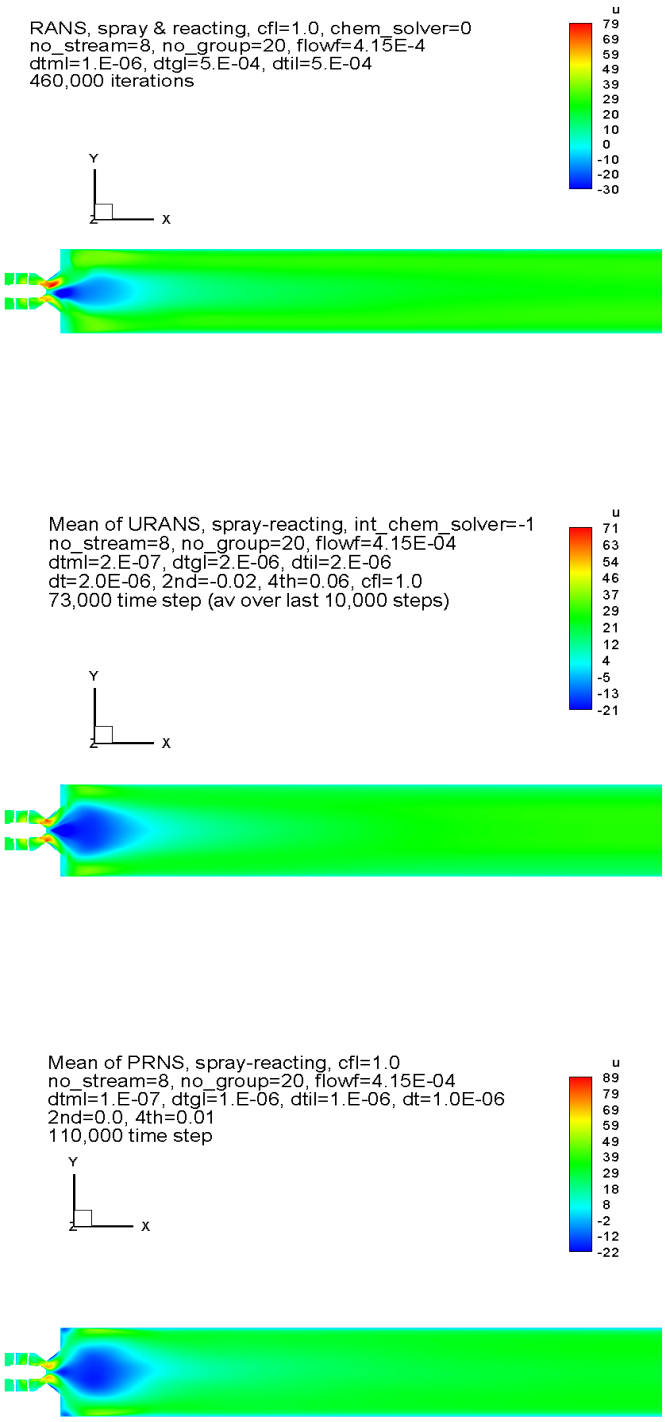

Figure 7.—Contours of the time averaged axial velocity in the center plane (well-mixed model): RANS, URANS, and PRNS.

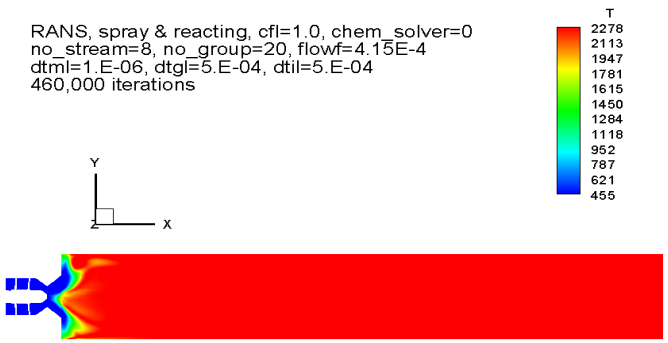

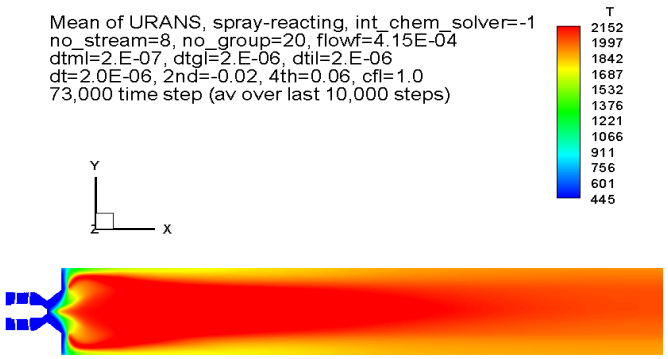

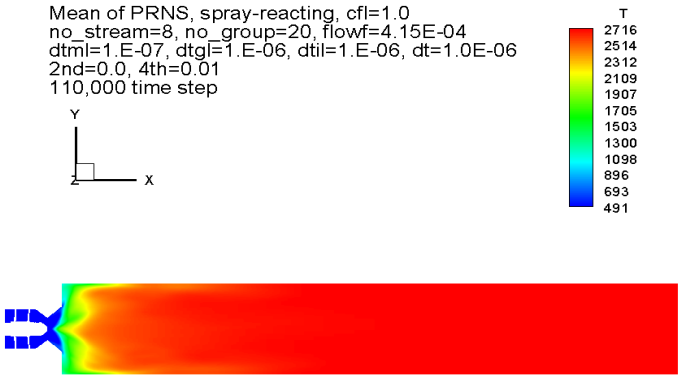

Figure 8.—Contours of the averaged temperature in the center plane (well-mixed model): RANS, URANS, and PRNS.

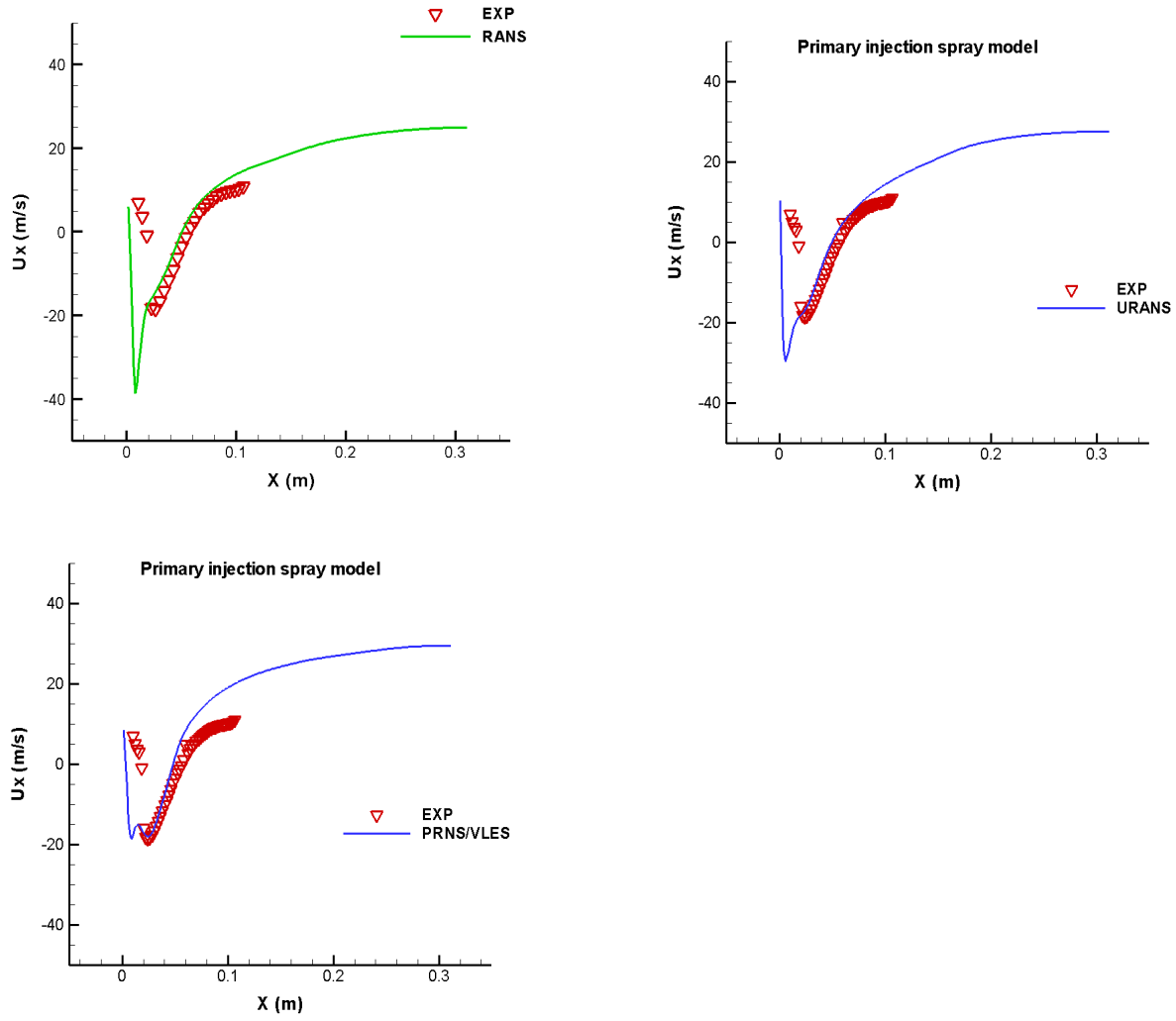

Figure 9.—Comparison of the time averaged axial velocity along the center line (well-mixed model): RANS, URANS, and PRNS.

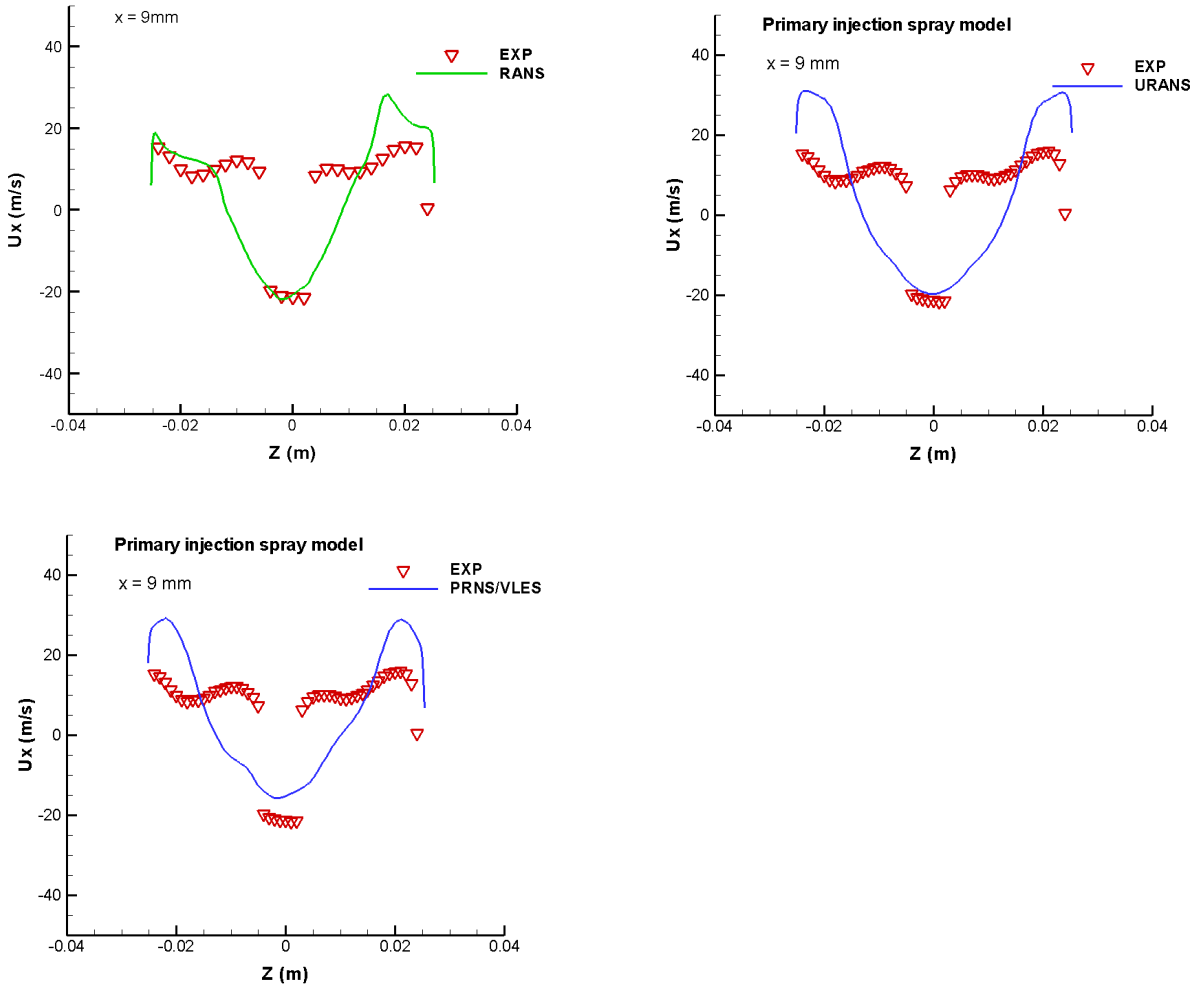

Figure 10.—Comparison of the time averaged axial velocity at x = 9 mm (well-mixed model): RANS, URANS, and PRNS.

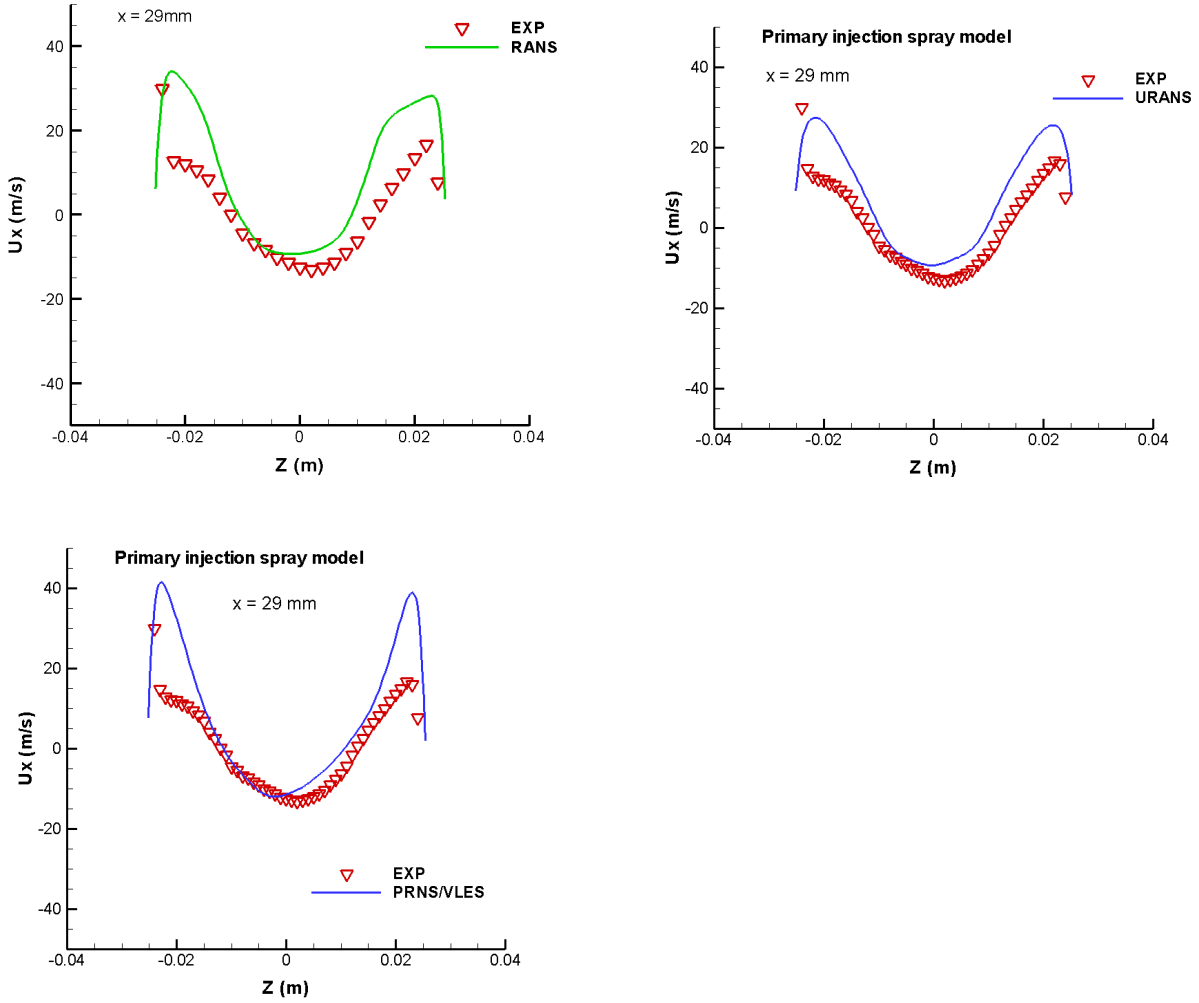

Figure 11.—Comparison of the time averaged axial velocity at x = 29 mm (well-mixed model): RANS, URANS, and PRNS.

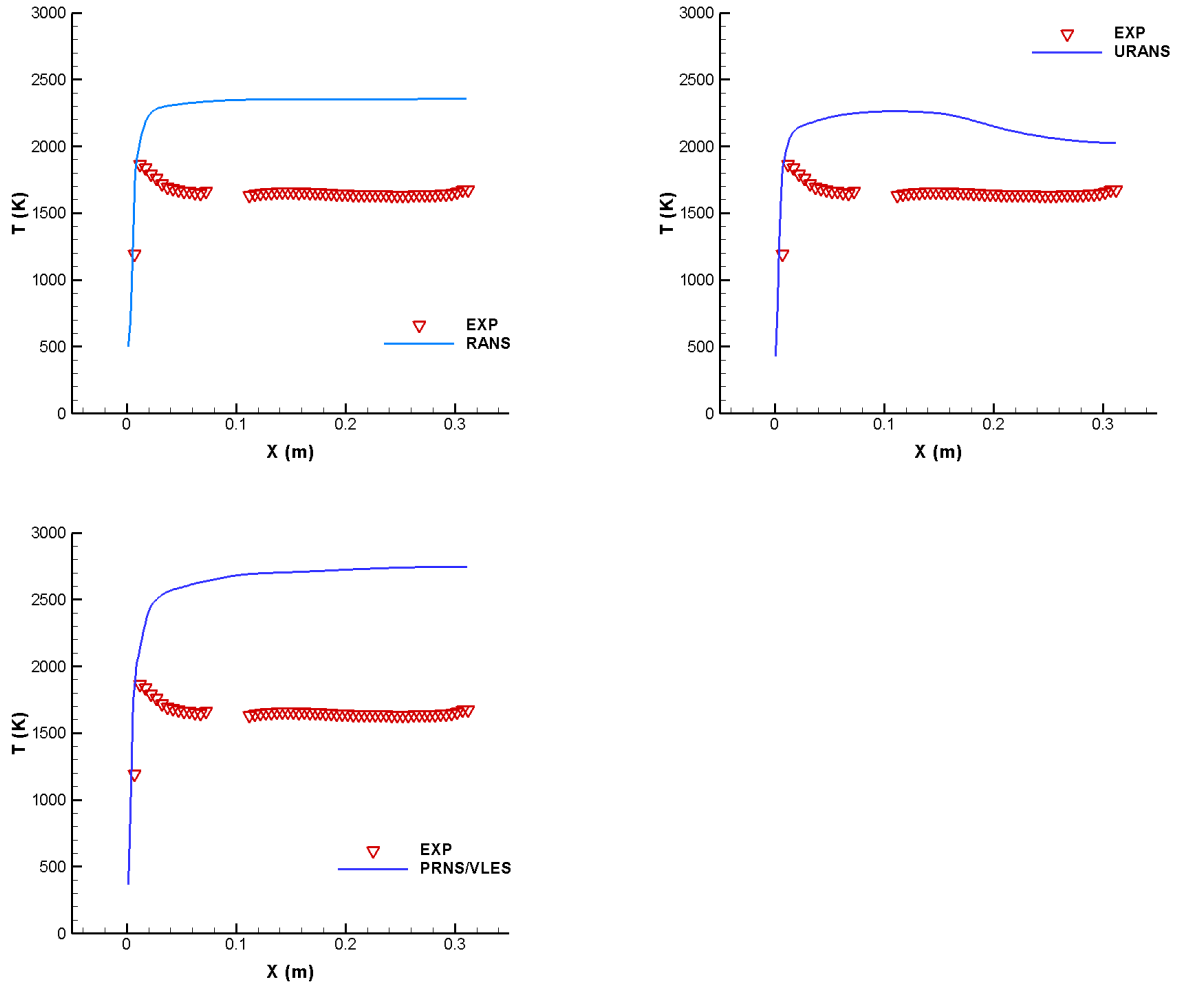

Figure 12.—Comparison of the time averaged temperature along the center line (well-mixed model): RANS, URANS, and PRNS.

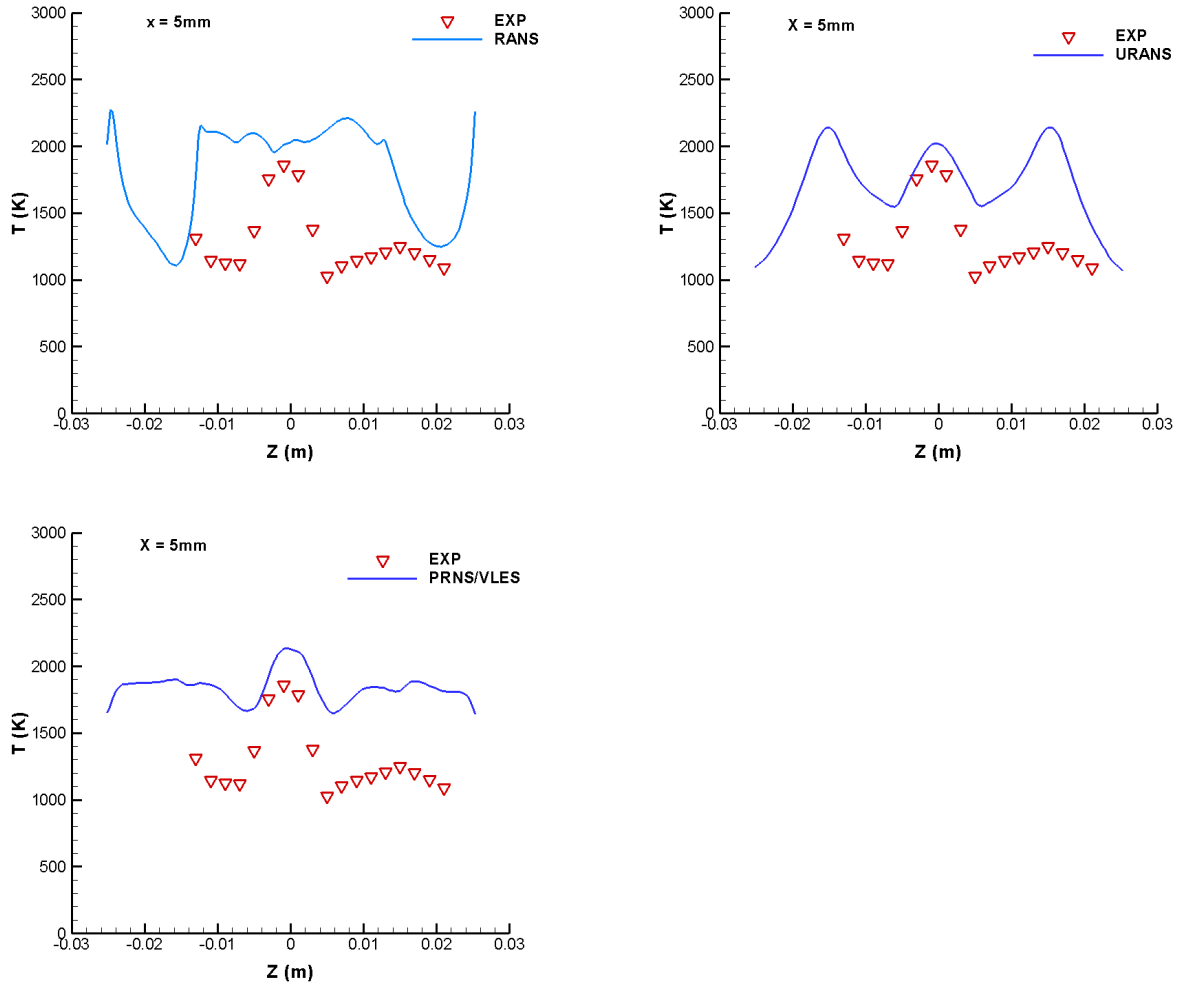

Figure 13.—Comparison of the time averaged temperature at x = 5 mm (well-mixed model): RANS, URANS, and PRNS.

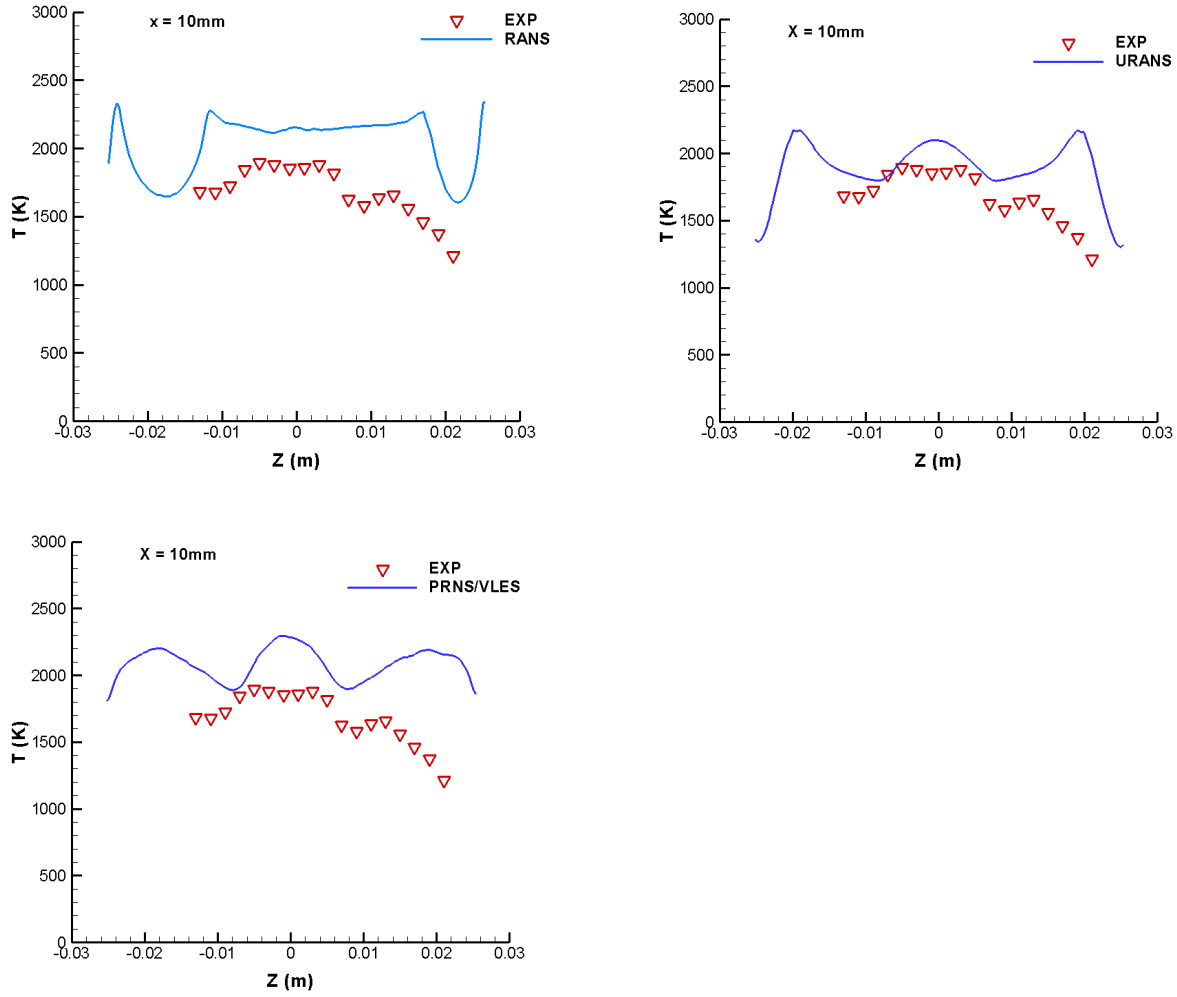

Figure 14.—Comparison of the time averaged temperature at x = 10 mm (well-mixed model): RANS, URANS, and PRNS.

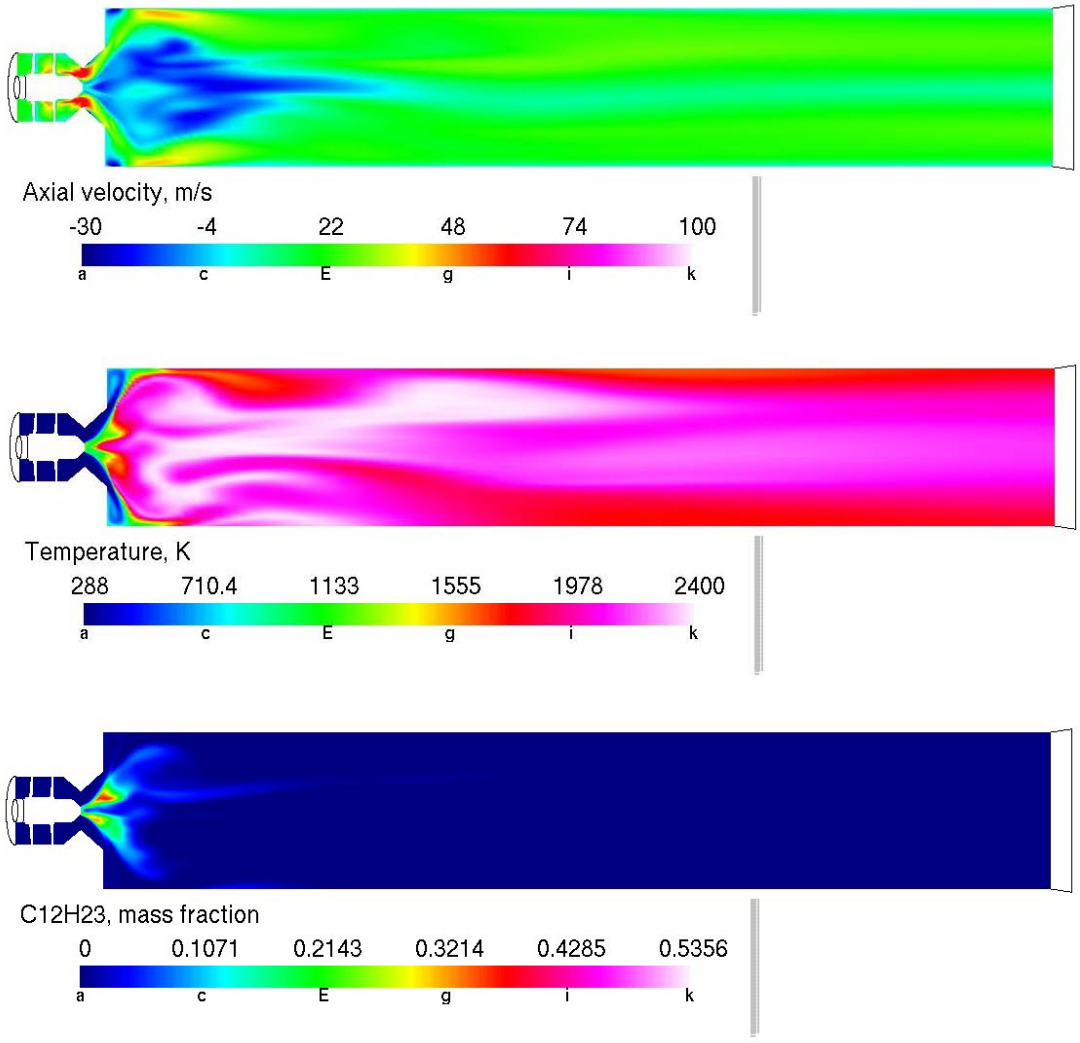

Figure 15.—Starting condition for LEM/PRNS and FDF/PRNS (in the center plane).

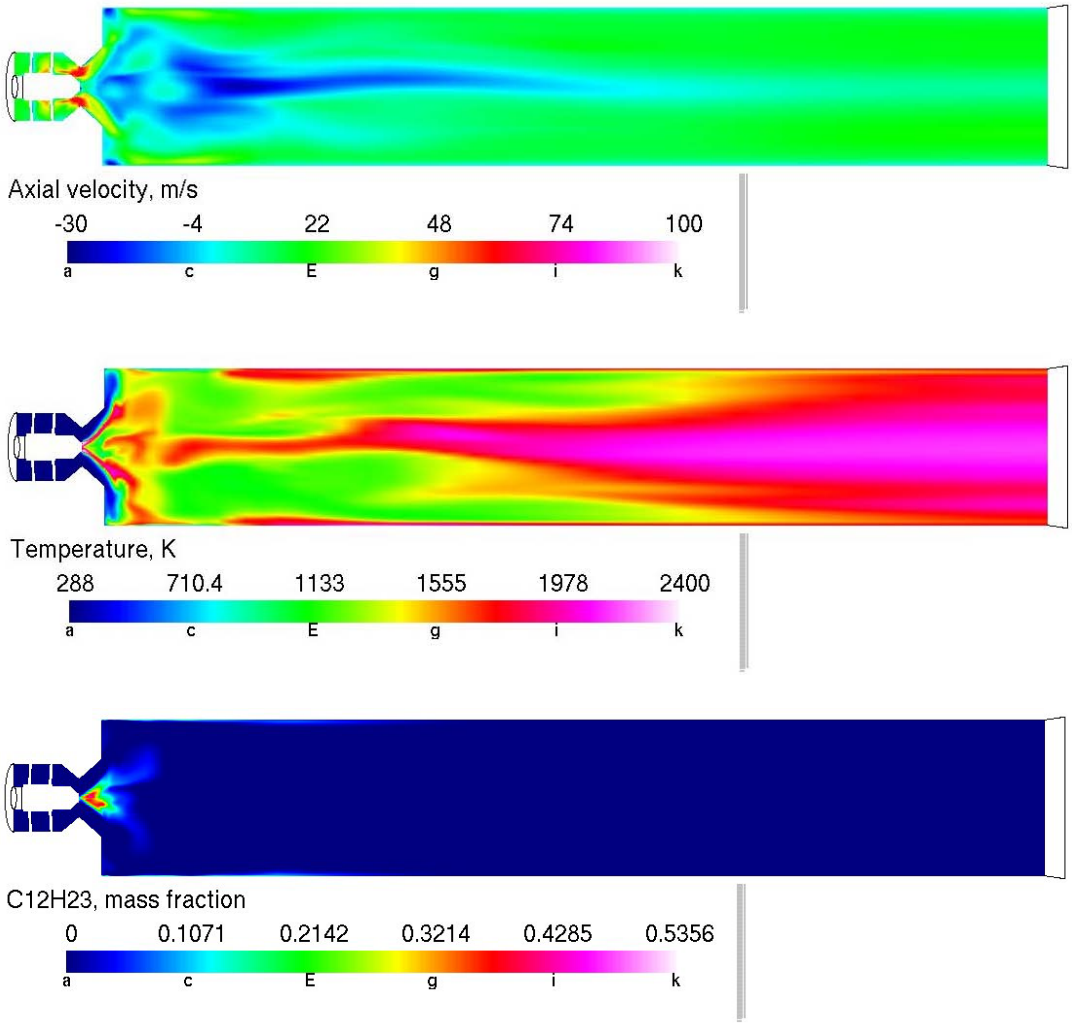

Figure 16.—LEM/PRNS time averaged contours in the center plane: axial velocity, temperature, and fuel vapor mass fraction.

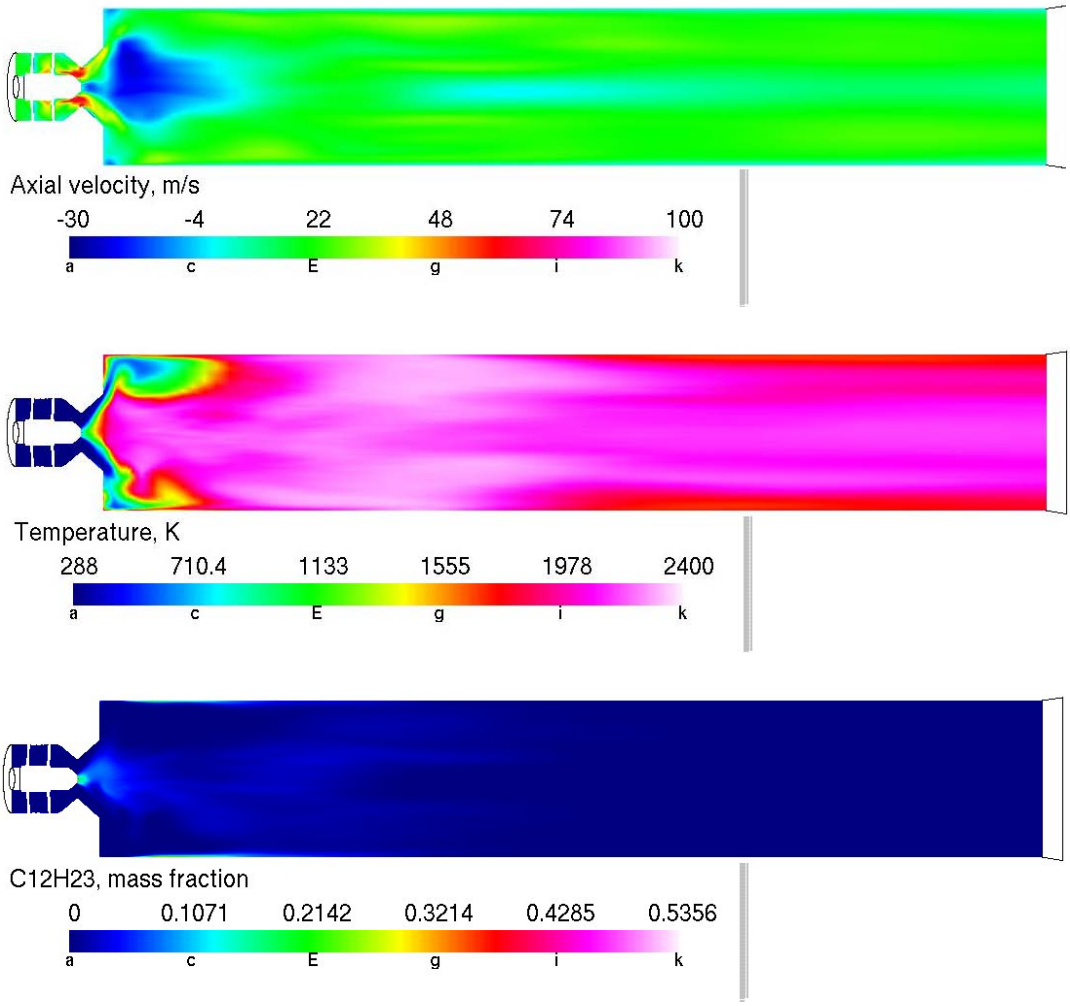

Figure 17.—FDF/PRNS time averaged contours in the center plane: axial velocity, temperature, and fuel vapor mass fraction.

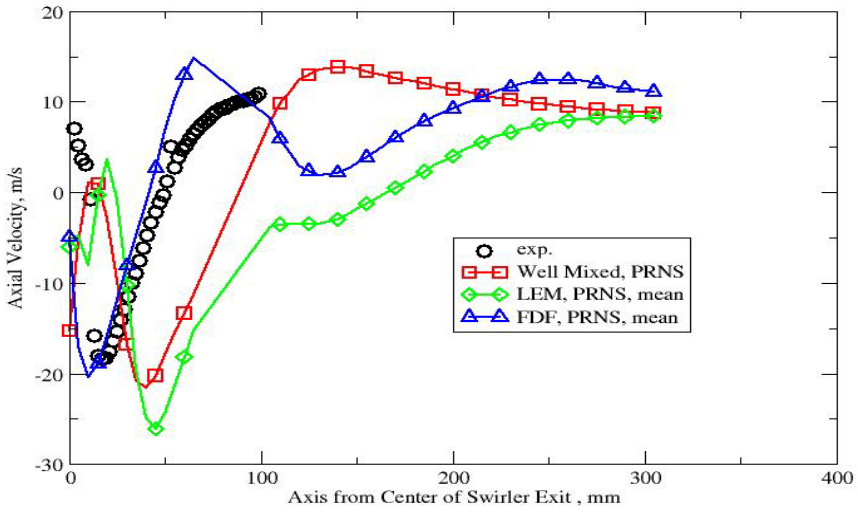

Figure 18.—Comparison of time averaged axial velocity along the center line (the instantaneous starting condition denoted as well-mixed/PRNS is included for reference).

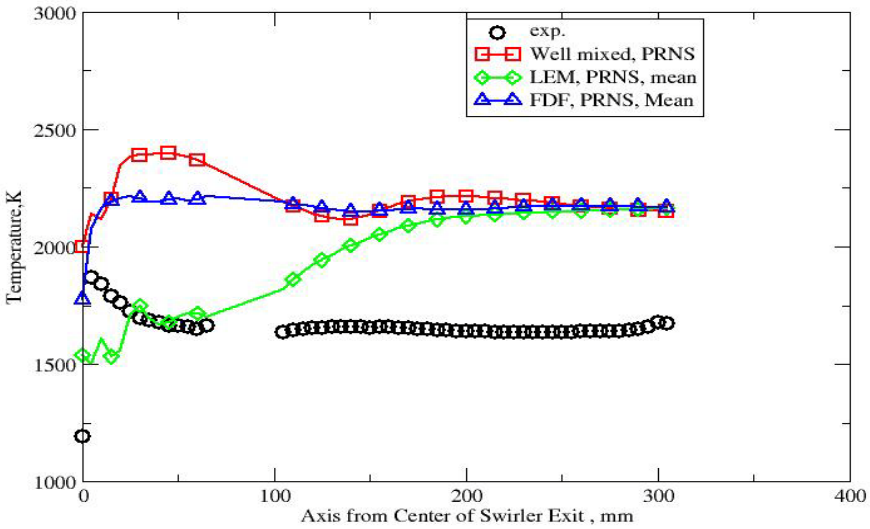

Figure 19.—Comparison of time averaged temperature along the center line (the instantaneous starting condition denoted as well-mixed/PRNS is included for reference).

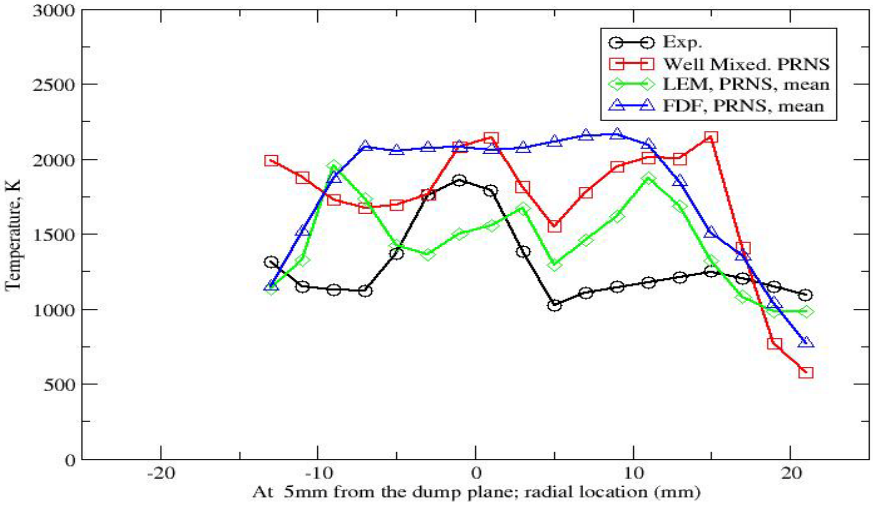

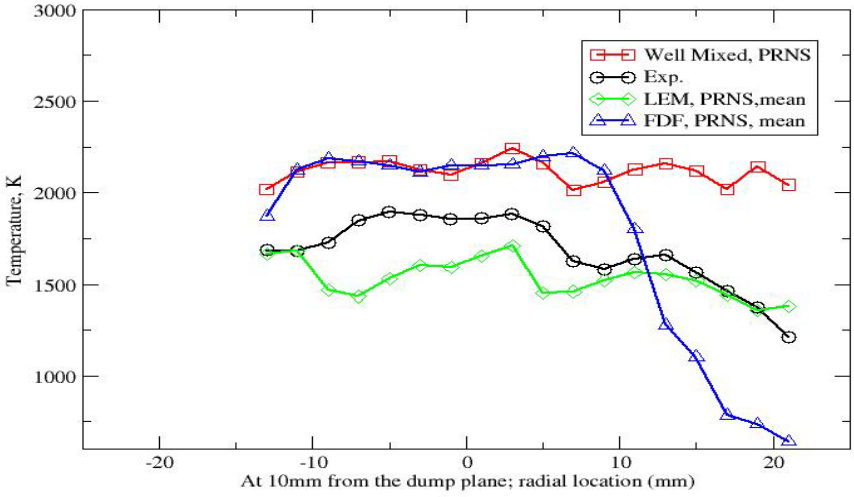

Figure 20.—Comparison of time averaged temperature at x = 5 mm, 10 mm (the instantaneous starting condition denoted as well-mixed/PRNS is included for reference).

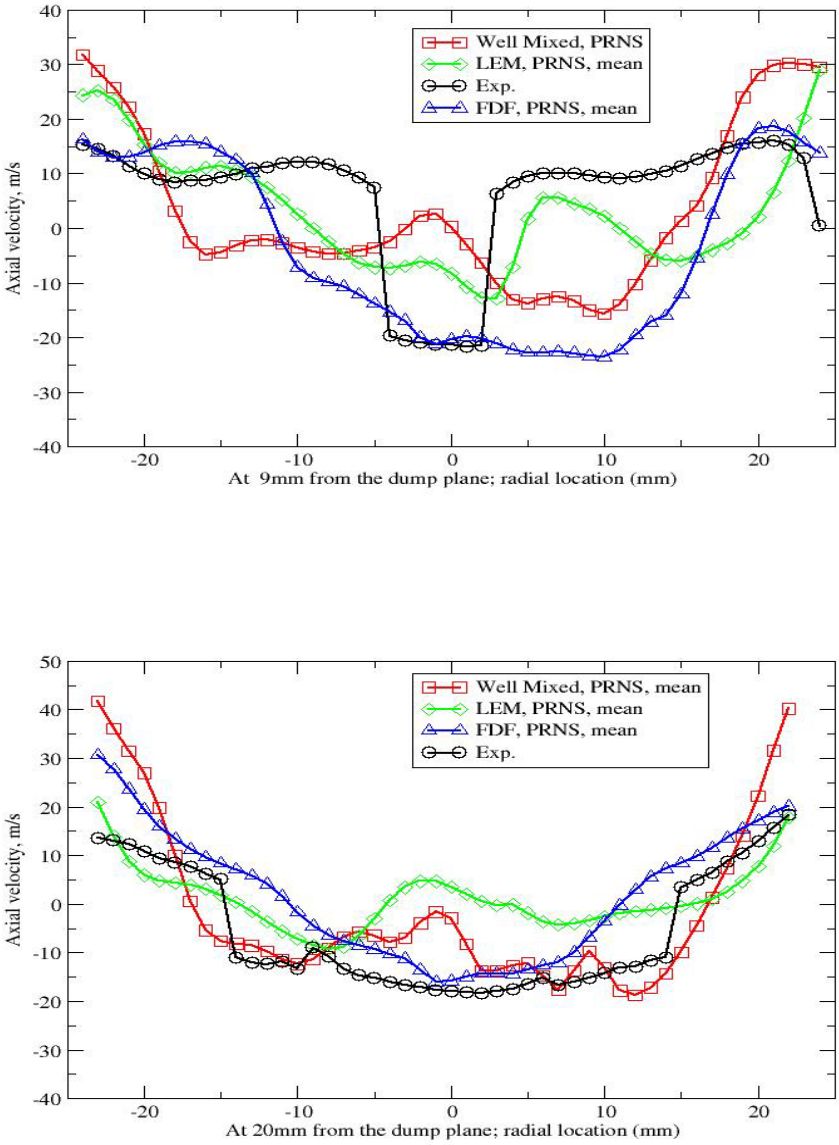

Figure 21.—Comparison of time averaged axial velocity at x = 9 mm, 20 mm (the instantaneous starting condition denoted as well-mixed/PRNS is included for reference).

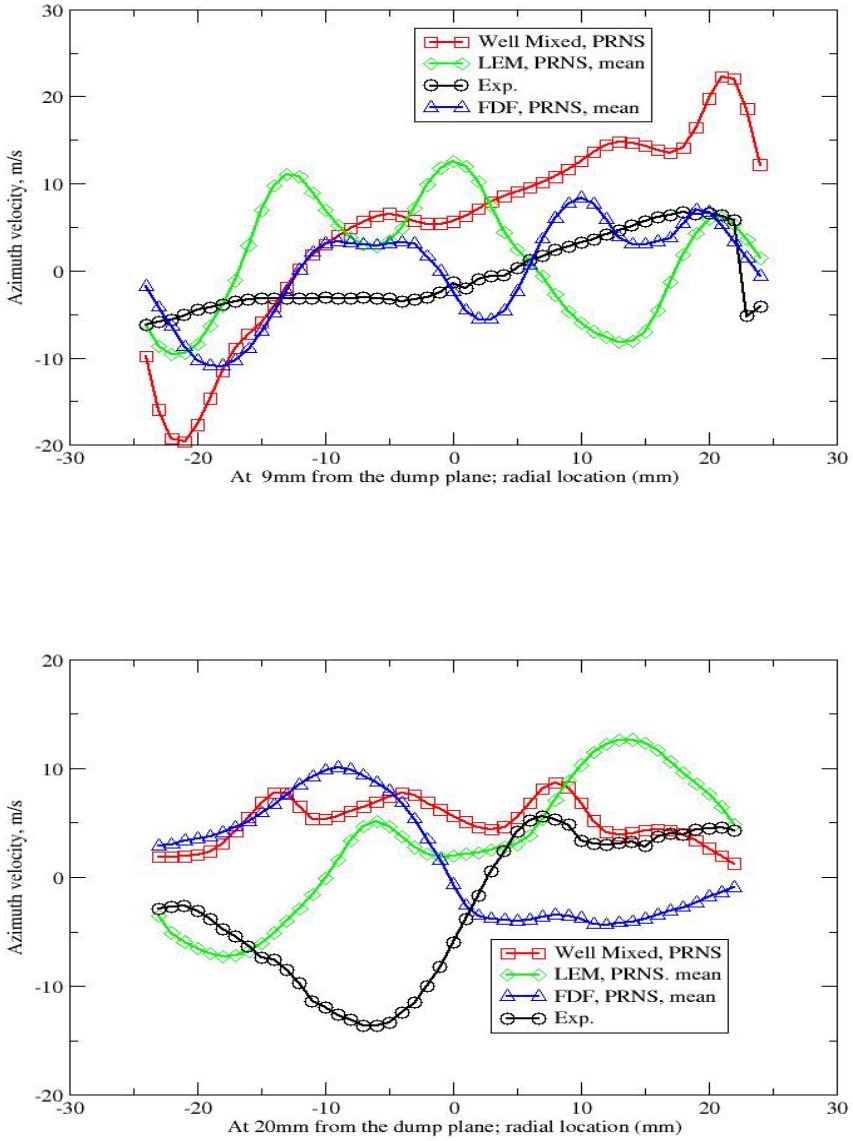

Figure 22.—Comparison of time averaged azimuth velocity at x = 9 mm, 20 mm (the instantaneous starting condition denoted as well-mixed/PRNS is included for reference).

REPORT DOCUMENTATION PAGE	Form Approved OMB No. 0704-0188

1. REPORT DATE *(DD-MM-YYYY)*	2. REPORT TYPE	3. DATES COVERED *(From - To)*
01-07-2011	Technical Memorandum	

4. TITLE AND SUBTITLE
Numerical Simulations of Two-Phase Reacting Flow in a Single-Element Lean Direct Injection (LDI) Combustor Using NCC

5a. CONTRACT NUMBER

5b. GRANT NUMBER

5c. PROGRAM ELEMENT NUMBER

6. AUTHOR(S)
Liu, Nan-Suey; Shih, Tsan-Hsing; Wey, C., Thomas

5d. PROJECT NUMBER

5e. TASK NUMBER

5f. WORK UNIT NUMBER
WBS 561581.02.08.03.16.02

7. PERFORMING ORGANIZATION NAME(S) AND ADDRESS(ES)
National Aeronautics and Space Administration
John H. Glenn Research Center at Lewis Field
Cleveland, Ohio 44135-3191

8. PERFORMING ORGANIZATION REPORT NUMBER
E-17725

9. SPONSORING/MONITORING AGENCY NAME(S) AND ADDRESS(ES)
National Aeronautics and Space Administration
Washington, DC 20546-0001

10. SPONSORING/MONITOR'S ACRONYM(S)
NASA

11. SPONSORING/MONITORING REPORT NUMBER
NASA/TM-2011-217031

12. DISTRIBUTION/AVAILABILITY STATEMENT
Unclassified-Unlimited
Subject Categories: 01 and 64
Available electronically at http://www.sti.nasa.gov
This publication is available from the NASA Center for AeroSpace Information, 443-757-5802

13. SUPPLEMENTARY NOTES

14. ABSTRACT
A series of numerical simulations of Jet-A spray reacting flow in a single-element lean direct injection (LDI) combustor have been conducted by using the National Combustion Code (NCC). The simulations have been carried out using the time filtered Navier-Stokes (TFNS) approach ranging from the steady Reynolds-averaged Navier-Stokes (RANS), unsteady RANS (URANS), to the dynamic flow structure simulation (DFS). The sub-grid model employed for turbulent mixing and combustion includes the well-mixed model, the linear eddy mixing (LEM) model, and the filtered mass density function (FDF/PDF) model. The starting condition of the injected liquid spray is specified via empirical droplet size correlation, and a five-species single-step global reduced mechanism is employed for fuel chemistry. All the calculations use the same grid whose resolution is of the RANS type. Comparisons of results from various models are presented.

15. SUBJECT TERMS
Combustion CFD

16. SECURITY CLASSIFICATION OF:			17. LIMITATION OF ABSTRACT	18. NUMBER OF PAGES	19a. NAME OF RESPONSIBLE PERSON
a. REPORT	b. ABSTRACT	c. THIS PAGE			STI Help Desk (email:help@sti.nasa.gov)
U	U	U	UU	34	19b. TELEPHONE NUMBER *(include area code)* 443-757-5802